


 Cite this: *Chem. Commun.*, 2020, 56, 9126

 Received 4th May 2020,  
 Accepted 2nd July 2020

DOI: 10.1039/d0cc03207g

rsc.li/chemcomm

# Surprisingly big linker-dependence of activity and selectivity in CO<sub>2</sub> reduction by an iridium(i) pincer complex†

 Gongfang Hu,<sup>†</sup> Jianbing “Jimmy” Jiang,<sup>‡\*c</sup> H. Ray Kelly,<sup>ab</sup> Adam J. Matula,<sup>ab</sup> Yueshen Wu,<sup>ab</sup> Neyen Romano,<sup>ab</sup> Brandon Q. Mercado,<sup>a</sup> Hailiang Wang,<sup>†</sup> Victor S. Batista,<sup>\*ab</sup> Robert H. Crabtree,<sup>†</sup> and Gary W. Brudvig,<sup>†\*</sup>

**Here, we report the quantitative electroreduction of CO<sub>2</sub> to CO by a PNP-pincer iridium(i) complex bearing amino linkers in DMF/water. The electrocatalytic properties greatly depend on the choice of linker within the ligand. The complex 3-N is far superior to the analogues with methylene and oxygen linkers, showing higher activity and better selectivity for CO<sub>2</sub> over proton reduction.**

The electroreduction of CO<sub>2</sub> to CO provides a pathway for conversion of electrical energy from renewable sources into liquid fuels and useful organic chemicals.<sup>1–6</sup> Despite notable progress in the development of several efficient CO<sub>2</sub> reduction catalysts (metals, metal oxides, organometallic complexes, and main-group compounds),<sup>1–5,7–15</sup> it remains challenging to improve the rate and selectivity of multielectron reduction reactions at low overpotentials.

Iridium complexes have been widely studied as efficient catalysts for the production of formate<sup>16–20</sup> and oxalate,<sup>21,22</sup> including a reported PNP-pincer Ir(III) complex **1** (Chart 1) for electrocatalytic CO<sub>2</sub> reduction to formate in acetonitrile/water,<sup>23</sup> an iridium trihydride complex **2** (Chart 1) for CO<sub>2</sub> conversion to formate,<sup>24</sup> and an Ir(III) hydride that gives predominant CO formation with 5–10% formate production.<sup>18</sup> However, to the best of our knowledge, an Ir catalyst for quantitative CO<sub>2</sub>-to-CO conversion has yet to be discovered. Here, we report a selective CO<sub>2</sub>-to-CO electroreduction by

a molecular Ir complex, without any detectable production of formate, or H<sub>2</sub>.

We observed surprising and unanticipated<sup>25</sup> differences in the catalytic selectivities for CO<sub>2</sub> electroconversion in the series of Ir(i) carbonyl pincer complexes **3-N**, **3-C**, and **3-O** (Chart 1). We find that the amino-linked **3-N** complex electrocatalytically reduces CO<sub>2</sub> to CO with 98% faradaic efficiency and a current density of 5.9 mA cm<sup>-2</sup> at -1.9 V vs. Ag/AgCl, without any significant production of formate or H<sub>2</sub>. However, the observed selectivity of CO over H<sub>2</sub> evolution diminishes to ~50% when the NH linkers are replaced by CH<sub>2</sub> groups (**3-C**). The oxygen linked complex **3-O** has drastically lower catalytic activity, we therefore analysed the origin of this unexpected variation in product selectivity at the density functional theory (DFT) level.

The preparation and characterization of complex **3-C** was previously reported,<sup>26</sup> while **3-N** and **3-O** were synthesized by cyclometallation of the corresponding pincer ligands with [IrCl(COE)<sub>2</sub>]<sub>2</sub> and [Ir(COE)<sub>2</sub>(acetone)<sub>2</sub>]PF<sub>6</sub> (COE = cyclooctene),<sup>27</sup> respectively, followed by ligand exchange with CO (Scheme S1, ESI†). The successful substitution of COE by CO was confirmed by the disappearance of the aliphatic protons of the COE ligand in the <sup>1</sup>H NMR spectrum and the appearance of IR bands at 1962 cm<sup>-1</sup> and 1980 cm<sup>-1</sup>. From the X-ray structure of **3-N**, the Ir lies out of the P,N,P plane by a mere 0.0186(12) Å; for **3-O** the metal lies in the plane and has a square planar coordination geometry (Fig. S2, ESI†).

The electrochemical properties of the complexes were investigated using cyclic voltammetry (CV) in aqueous DMF (5 M H<sub>2</sub>O)

<sup>a</sup> Department of Chemistry, Yale University, New Haven, Connecticut, 06520, USA. E-mail: victor.batista@yale.edu, hailiang.wang@yale.edu, gary.brudvig@yale.edu

<sup>b</sup> Energy Sciences Institute, Yale University, West Haven, Connecticut, 06516, USA

<sup>c</sup> Department of Chemistry, University of Cincinnati, P.O. Box 210172, Cincinnati, Ohio 45221-0172, USA. E-mail: jianbing.jiang@uc.edu

† Electronic supplementary information (ESI) available: Experimental details; cyclic voltammetry, UV-Vis spectra, and FT-IR spectra of complex **3-zN**, **3-C**, and **3-O**; XRD of complex **3-N** and **3-O**. Foot-of-wave analysis and kinetic analysis of **3-N**; SEM, EDS, and XPS analysis of activated surface; calculation details and results; crystal data of **3-N**; and crystal data of **3-O**. CCDC 2001541 and 2001542. For ESI and crystallographic data in CIF or other electronic format see DOI: 10.1039/d0cc03207g

‡ These authors contributed equally to this work.

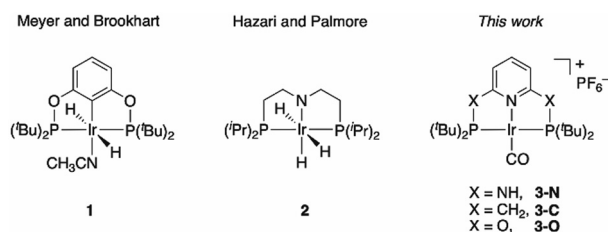


Chart 1 Iridium complexes for CO<sub>2</sub> reduction studied before and here.

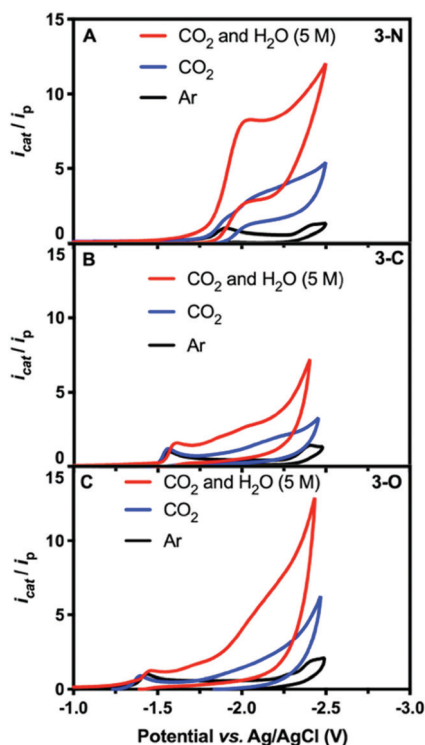


Fig. 1 CV scans of 0.5 mM solutions of **3-N** (A), **3-C** (B), and **3-O** (C) in DMF under argon (black), CO<sub>2</sub> (blue), and CO<sub>2</sub> with 5 M H<sub>2</sub>O (red).

with glassy carbon as the working electrode and 0.1 M [<sup>n</sup>Bu<sub>4</sub>N][PF<sub>6</sub>] as the supporting electrolyte. Under argon, the CV of **3-N** shows the first irreversible reduction peak at  $-1.91$  V, and the second at  $-2.39$  V (Fig. 1A and Fig. S3, ESI<sup>†</sup>). All potentials are listed versus Ag/AgCl (see ESI<sup>†</sup>). DFT calculations predicted successive one-electron reductions at  $-1.93$  V and  $-2.39$  V vs. Ag/AgCl, in excellent agreement with our measurements (Fig. S4, ESI<sup>†</sup>). The plots of peak current versus square root of the scan rate are linear, as expected for a diffusion-controlled process (inset in Fig. S5, ESI<sup>†</sup>).

Catalytic CO<sub>2</sub> electroreduction of **3-N** was identified by comparing CV measurements in DMF under Ar with those under CO<sub>2</sub> both with and without 5 M water as the proton source. Fig. 1 shows the normalized current  $i_{cat}/i_p$ , where  $i_p$  is the peak current for the first reduction for each species under argon, and  $i_{cat}$  is the measured catalytic current. In CO<sub>2</sub>-saturated dry DMF, a cathodic current increase is observed at ( $i_{cat}/i_p = 4.3$ ),<sup>28</sup> along with a 100 mV cathodic shift of the peak potential to  $-2.01$  V (Fig. 1A, blue). The cathodic shift in the reduction potential indicates substrate binding to **3-N**. Further CV measurements in the presence of CO<sub>2</sub> and water (5 M) afforded a significant catalytic current ( $i_{cat}/i_p = 8.7$ ), corresponding to CO<sub>2</sub> reduction (Fig. 1A, red). The overpotential was estimated to be 0.86 V, using the half-wave potential ( $-1.89$  V vs. Ag/AgCl) and the thermodynamic potential for CO<sub>2</sub>-to-CO conversion in DMF/H<sub>2</sub>O mixture from the literature<sup>29,30</sup> (see ESI<sup>†</sup>). Attempts at determining the observed rate constant  $k_{obs}$  and turnover frequency through foot-of-the-wave analysis<sup>29,31,32</sup> resulted in plots with significant nonlinearity (Fig. S6, ESI<sup>†</sup>). We defer mechanistic work to the full paper, but this could possibly indicate a mechanism with

electron transfer followed by a chemical step (ECEC), with a rapid first chemical step for CO<sub>2</sub> reduction.<sup>33,34</sup> No catalytic current independent of scan rate could be measured under CO<sub>2</sub>-saturated DMF/H<sub>2</sub>O mixture. Further insight was gained through CV measurements of **3-N** under various concentrations of CO<sub>2</sub> and water. Under pseudo-first-order conditions, **3-N** displays a first-order dependence on CO<sub>2</sub> concentration but exhibits deviation from linearity at lower concentrations, presumably as a result of local depletion of CO<sub>2</sub> (Fig. S7, ESI<sup>†</sup>). A pseudo-first-order dependence was observed for **3-N** upon variation of the water concentration (Fig. S8, ESI<sup>†</sup>).

Conversely, **3-C** and **3-O** showed irreversible but more anodic reduction potentials under argon, at  $-1.57$  V (Fig. 1B and Fig. S9, ESI<sup>†</sup>) and  $-1.44$  V (Fig. 1C and Fig. S10, ESI<sup>†</sup>), respectively. No significant current increase was observed for either complex in the presence of CO<sub>2</sub>, with or without water at their first reduction potentials, indicating a far lower catalytic activity.

Controlled-potential electrolysis (CPE) of the three complexes at various potentials was performed for electrochemical CO<sub>2</sub> reduction in DMF with 5 M water, using high-surface-area carbon fibre paper as the working electrode. At all relevant potentials, only CO and H<sub>2</sub> were detected with no liquid products (Fig. S11, ESI<sup>†</sup>). The faradaic efficiency for CO and total current density of **3-N** at various potentials are shown in Fig. 2A. More negative potentials led to higher CO faradaic efficiencies and total current densities. The highest faradaic efficiency for CO of 98% was achieved at  $-2.00$  V, where the total current density was  $7.8$  mA cm<sup>-2</sup>. The lowest potential with a similarly high CO faradaic efficiency ( $-1.90$  V) was selected for long-term CPE. High CO faradaic efficiency (98%) and total current density ( $5.8$  mA cm<sup>-2</sup>) were maintained for over 67 hours (Fig. 2D), demonstrating the excellent stability of catalyst **3-N**. Complex **3-C** exhibited activity for CO<sub>2</sub> reduction ( $\sim 3.8$  mA cm<sup>-2</sup>) at  $-1.70$  V. However, H<sub>2</sub> evolution was significant for **3-C**, resulting in an approximately 1:1 mixture of CO/H<sub>2</sub> from  $-1.70$  to  $-2.00$  V (Fig. 2B). CPE using **3-O** under the same electrocatalytic conditions showed little catalytic activity for either CO<sub>2</sub> or H<sup>+</sup> reduction (Fig. 2C). The smaller current density ( $\sim 1.8$  mA cm<sup>-2</sup> at  $-2.00$  V) and low CO production efficiency ( $< 25\%$ ) are consistent with the background activity generated by the carbon paper electrode.<sup>35</sup>

UV-Vis spectra of the electrolyte solutions were recorded before and after electrolysis (Fig. S13 and S14, ESI<sup>†</sup>) to confirm that molecular integrity of complex **3-N** is retained and that no metal dissociation occurred during CPE. The two spectra are nearly identical, indicating that ligand degradation and demetallation are insignificant during CPE. Scanning Electron Microscopy (SEM), Energy Dispersive X-ray Spectroscopy (EDS) and X-ray Photoelectron Spectroscopy (XPS) were performed on the carbon fibre paper after CPE (Fig. S15–S17, ESI<sup>†</sup>). The absence of an iridium signal in either the EDS or XPS spectra suggests no significant iridium demetallation at the carbon electrode. The carbon electrode of **3-N** was gently washed with DMF after CPE and used again as the working electrode in a fresh electrolyte solution (DMF with 5 M water) without **3-N**. No

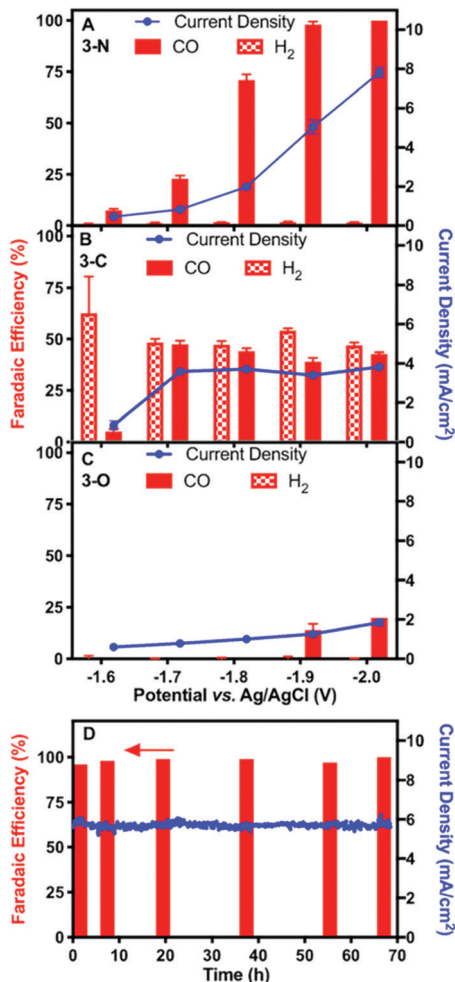


Fig. 2 CO and H<sub>2</sub> faradaic efficiencies and total current densities at various potentials for complexes **3-N** (A), **3-C** (B), and **3-O** (C) at a concentration of 0.5 mM in DMF with 5 M water. Error bars represent standard errors from three successive measurements at the same potentials. (D) CO faradaic efficiencies after 2, 6, 20, 37, 55, and 67 hours and total current density during CPE of **3-N** at  $-1.90$  V. Electrolyses were performed using a carbon paper electrode with a 1 cm<sup>2</sup> geometric area as the working electrode.

CO<sub>2</sub> reduction product was detected, further confirming that the active species for CO<sub>2</sub> reduction is homogeneous **3-N**, rather than its heterogenized form, or deposited iridium metal.

The electronic properties of the three complexes, before and after reduction, were analysed by DFT calculations that provided insights into the origin of the unexpected changes in catalytic activity and selectivity induced by the change of linker. The calculations reproduced the experimental trends in carbonyl stretching frequencies (Table S2, ESI<sup>†</sup>) and the reduction potentials for the three complexes (Table S3, ESI<sup>†</sup>). The calculated one-electron reduction potentials,  $-1.93$  V for **3-N**,  $-1.81$  V for **3-C**, and  $-1.67$  V for **3-O**, are in good agreement with the experimental potentials. As expected, the trend in reduction potentials correlates with the relative LUMO energies of the three complexes, with higher energy LUMOs corresponding to more negative reduction potentials (Fig. 3). A relationship between LUMO energies and

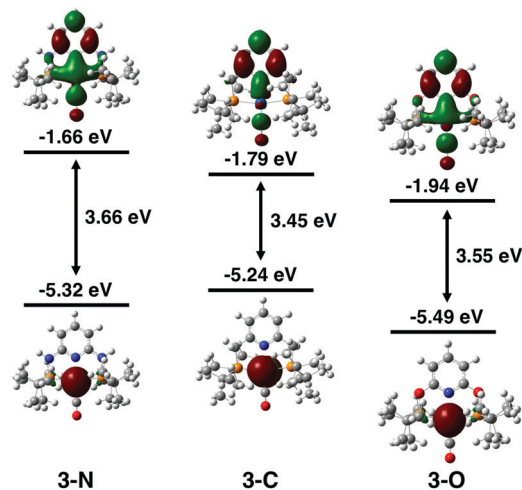


Fig. 3 DFT calculated HOMO and LUMO energy levels of **3-N** (left), **3-C** (middle), and **3-O** (right). **3-N** has the highest energy LUMO despite having a lower HOMO energy than **3-C**. This high-energy LUMO is correlated with the more negative reduction potential of **3-N**.

electron affinity follows from Koopmans' theorem,<sup>36</sup> and a linear correlation between DFT LUMO energies and reduction potentials has previously been demonstrated.<sup>37</sup> For all three complexes, the HOMOs are centred on the Ir, while the LUMOs are delocalized over the ligand and metal centre (Fig. S21, ESI<sup>†</sup>). The LUMO of **3-N** has more Ir character, suggesting that the reduction is predominantly centred on the metal.

DFT calculations shed light on the effect of reduction. The comparison of spin densities in the reduced complexes (Fig. 4) reveals that the unpaired electron in **3-N** is most localized on the Ir centre. This may be the key factor that makes **3-N** more reactive than the other complexes in the series for CO<sub>2</sub> reduction. The SOMOs of the reduced complexes (Fig. S22, ESI<sup>†</sup>) and corresponding spin population analysis (Fig. S23 and Table S4, ESI<sup>†</sup>) further support the idea that the Ir centre of **3-N** is more affected upon reduction than those of **3-C**, or **3-O**. In all cases, the linker atoms themselves have negligible spin population, suggesting that the linker substitution alters the reactivity by tuning the electronic properties of the ligand. Additionally, electron density

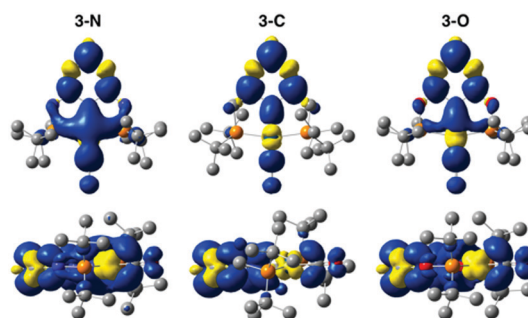


Fig. 4 Spin density on reduced complexes **3-N** (left), **3-C** (middle), and **3-O** (right). Blue and yellow surfaces (isovalue = 0.001) indicate excess alpha and beta spin densities, respectively. Hydrogen atoms have been omitted from the structures for clarity.

difference plots (Fig. S24, ESI<sup>†</sup>) show that 3-N has the largest increase in electron density at the metal centre after reduction. Before reduction, 3-C has the most electron density on the Ir consistent with the experimental and calculated CO stretching frequencies (Table S2, ESI<sup>†</sup>) and CM5 partial charges (Table S5, ESI<sup>†</sup>).<sup>38</sup> After reduction, 3-N has the more electron density on the Ir, and corresponding lower CO stretching frequency and more negative partial charge on the Ir atom than for the other members of the series. Taken together, these calculations suggest that the linker atoms modulate the electron density at the catalytic centre by tuning the electronic properties of the ligand.

In summary, we find that the electrocatalytic properties of a series of three pincer-iridium(i) complexes are strongly modulated by the nature of the ligand. Complex 3-N with amino linkers in the pincer ligand exhibited prolonged stability and nearly quantitative efficiency for CO<sub>2</sub>-to-CO conversion, with no significant proton reduction observed with a half-wave overpotential about 0.86 V. The complex remained molecular throughout the course of electrolysis. Replacing the amino linker with a methylene group resulted in complex 3-C, with poor selectivity, while replacing the amino group by an oxygen unit leads to 3-O which has no significant catalytic activity. DFT calculations suggest that 3-N is most active possibly because of the highest electron density on the iridium centre after reduction, leading to a more active catalytic centre for CO<sub>2</sub> reduction. Increased electron density at the metal centre has previously been shown to result in higher activities and increased faradaic efficiency for CO production.<sup>39,40</sup> In-depth mechanistic studies are in progress. These results suggest that variation of the linkers in pincer ligands can strongly affect the catalytic performance by modulating the spin density on the CO<sub>2</sub> binding site and could thus be exploited for ligand screening in computational catalyst design.<sup>41</sup>

We thank the staff at the Yale West Campus Analytical Core and the Yale Chemical and Biophysical Instrumentation Centre for their help with the instrumentation. This work was supported by the U.S. Department of Energy, Chemical Sciences, Geosciences, and Biosciences Division, Office of Basic Energy Sciences, Office of Science (Grant DEFG02-07ER15909) and partly by the U.S. National Science Foundation (grant CHE-1651717). Additional support was provided by a generous donation from the TomKat Charitable Trust. V. S. B. acknowledges computational time from NERSC and Yale HPC.

## Conflicts of interest

There are no conflicts to declare.

## Notes and references

- 1 A. J. Morris, G. J. Meyer and E. Fujita, *Acc. Chem. Res.*, 2009, **42**, 1983.
- 2 J.-M. Savéant, *Chem. Rev.*, 2008, **108**, 2348.

- 3 R. B. Ambre, Q. Daniel, T. Fan, H. Chen, B. Zhang, L. Wang, M. S. G. Ahlquist, L. Duan and L. Sun, *Chem. Commun.*, 2016, **52**, 14478.
- 4 R. Francke, B. Schille and M. Roemelt, *Chem. Rev.*, 2018, **118**, 4631.
- 5 M. G. Kibria, J. P. Edwards, C. M. Gabardo, C.-T. Dinh, A. Seifitokaldani, D. Sinton and E. H. Sargent, *Adv. Mater.*, 2019, **31**, 1807166.
- 6 C. Hepburn, E. Adlen, J. Beddington, E. A. Carter, S. Fuss, N. M. Dowell, J. C. Minx, P. Smith and C. K. Williams, *Nature*, 2019, **575**, 87.
- 7 C. Costentin, M. Robert and J.-M. Savéant, *Chem. Soc. Rev.*, 2013, **42**, 2423.
- 8 J. Qiao, Y. Liu, F. Hong and J. Zhang, *Chem. Soc. Rev.*, 2014, **43**, 631.
- 9 X. Duan, J. Xu, Z. Wei, J. Ma, S. Guo, S. Wang, H. Liu and S. Dou, *Adv. Mater.*, 2017, **29**, 1701784.
- 10 N. Elgrishi, M. B. Chambers, X. Wang and M. Fontecave, *Chem. Soc. Rev.*, 2017, **46**, 761.
- 11 H. Takeda, C. Cometto, O. Ishitani and M. Robert, *ACS Catal.*, 2017, **7**, 70.
- 12 F. Franco, S. Fernández and J. Lloret-Fillol, *Curr. Opin. Electrochem.*, 2019, **15**, 109.
- 13 K. E. Dalle, J. Warnan, J. J. Leung, B. Reuillard, I. S. Karmel and E. Reisner, *Chem. Rev.*, 2019, **119**, 2752.
- 14 C. Jiang, A. W. Nichols and C. W. Machan, *Dalton Trans.*, 2019, **48**, 9454–9468.
- 15 D. Gao, R. M. Aran-Ais, H. S. Jeon and B. R. Cuenya, *Nat. Catal.*, 2019, **2**, 198.
- 16 P. Kang, S. Zhang, T. J. Meyer and M. Brookhart, *Angew. Chem., Int. Ed.*, 2014, **53**, 8709.
- 17 A. Szymaszek and F. P. Pruchnik, *J. Organomet. Chem.*, 1989, **376**, 133.
- 18 G. F. Manbeck, K. Garg, T. Shimoda, D. J. Szalda, M. Z. Ertem, J. T. Muckerman and E. Fujita, *Faraday Discuss.*, 2017, **198**, 301.
- 19 F. D. Sypaseuth, C. Matlachowski, M. Weber, M. Schwalbe and C. C. Tzschucke, *Chem. – Eur. J.*, 2015, **21**, 6564.
- 20 P. Kang, T. J. Meyer and M. Brookhart, *Chem. Sci.*, 2013, **4**, 3497.
- 21 K. Tanaka, Y. Kushi, K. Tsuge, K. Toyohara, T. Nishioka and K. Isobe, *Inorg. Chem.*, 1998, **37**, 120.
- 22 Y. Kushi, H. Nagao, T. Nishioka, K. Isobe and K. Tanaka, *J. Chem. Soc., Chem. Commun.*, 1995, 1223.
- 23 P. Kang, C. Cheng, Z. Chen, C. K. Schauer, T. J. Meyer and M. Brookhart, *J. Am. Chem. Soc.*, 2012, **134**, 5500.
- 24 S. T. Ahn, E. A. Bielinski, E. M. Lane, Y. Chen, W. H. Bernskoetter, N. Hazari and G. T. R. Palmore, *Chem. Commun.*, 2015, **51**, 5947.
- 25 E. Peris and R. H. Crabtree, *Chem. Soc. Rev.*, 2018, **47**, 1959.
- 26 S. M. Kloek, D. M. Heinekey and K. I. Goldberg, *Organometallics*, 2006, **25**, 3007.
- 27 R. Dorta, R. Goikhman and D. Milstein, *Organometallics*, 2003, **22**, 2806.
- 28 B. P. Sullivan, C. M. Bolinger, D. Conrad, W. J. Vining and T. J. Meyer, *J. Chem. Soc., Chem. Commun.*, 1985, 1414.
- 29 C. Costentin, S. Drouet, M. Robert and J.-M. Savéant, *J. Am. Chem. Soc.*, 2012, **134**, 11235.
- 30 Y. Matsubara, *ACS Energy Lett.*, 2019, **4**, 1999.
- 31 C. Costentin and J.-M. Savéant, *ChemElectroChem*, 2014, **1**, 1226.
- 32 E. S. Rountree, B. D. McCarthy, T. T. Eisenhart and J. L. Dempsey, *Inorg. Chem.*, 2014, **53**, 9983.
- 33 V. C.-C. Wang and B. A. Johnson, *ACS Catal.*, 2019, **9**, 7109.
- 34 E. S. Wiedner, H. J. S. Brown and M. L. Helm, *J. Am. Chem. Soc.*, 2016, **138**, 604.
- 35 Y. Wu, J. Jiang, Z. Weng, M. Wang, D. L. J. Broere, Y. Zhong, G. W. Brudvig, Z. Feng and H. Wang, *ACS Cent. Sci.*, 2017, **3**, 847.
- 36 T. Koopmans, *Physica*, 1934, **1**, 104.
- 37 D. D. Méndez-Hernández, P. Tarakeshwar, D. Gust, T. A. Moore, A. L. Moore and V. Mujica, *J. Mol. Model.*, 2013, **19**, 2845.
- 38 A. V. Marenich, S. V. Jerome, C. J. Cramer and D. G. Truhlar, *J. Chem. Theory Comput.*, 2012, **8**, 527.
- 39 M. L. Clark, P. L. Cheung, M. Lessio, E. A. Carter and C. P. Kubiak, *ACS Catal.*, 2018, **8**, 2021.
- 40 J. A. Therrien and M. O. Wolf, *Inorg. Chem.*, 2017, **56**, 1161.
- 41 J. G. Freeze, H. R. Kelly and V. S. Batista, *Chem. Rev.*, 2019, **119**, 6595–6612.